RESEARCH ARTICLE

CORONAVIRUS

SARS-CoV-2 productively infects human gut enterocytes

Mart M. Lamers[1]*, Joep Beumer[2]*, Jelte van der Vaart[2]*, Kèvin Knoops[3], Jens Puschhof[2], Tim I. Breugem[1], Raimond B. G. Ravelli[3], J. Paul van Schayck[3], Anna Z. Mykytyn[1], Hans Q. Duimel[3], Elly van Donselaar[3], Samra Riesebosch[1], Helma J. H. Kuijpers[3], Debby Schipper[1], Willine J. van de Wetering[3], Miranda de Graaf[1], Marion Koopmans[1], Edwin Cuppen[4,5], Peter J. Peters[3], Bart L. Haagmans[1]†, Hans Clevers[2]†‡

Severe acute respiratory syndrome coronavirus 2 (SARS-CoV-2) can cause coronavirus disease 2019 (COVID-19), an influenza-like disease that is primarily thought to infect the lungs with transmission through the respiratory route. However, clinical evidence suggests that the intestine may present another viral target organ. Indeed, the SARS-CoV-2 receptor angiotensin-converting enzyme 2 (ACE2) is highly expressed on differentiated enterocytes. In human small intestinal organoids (hSIOs), enterocytes were readily infected by SARS-CoV and SARS-CoV-2, as demonstrated by confocal and electron microscopy. Enterocytes produced infectious viral particles, whereas messenger RNA expression analysis of hSIOs revealed induction of a generic viral response program. Therefore, the intestinal epithelium supports SARS-CoV-2 replication, and hSIOs serve as an experimental model for coronavirus infection and biology.

Severe acute respiratory syndrome (SARS), caused by the coronavirus SARS-CoV, emerged in 2003 (*1*). In late 2019, a novel transmissible coronavirus, SARS-coronavirus 2 (SARS-CoV-2), was noted to cause an influenza-like disease ranging from mild respiratory symptoms to severe lung injury, multiorgan failure, and death (*2*–*4*). SARS-CoV and SARS-CoV-2 belong to the *Sarbecovirus* subgenus of the genus *Betacoronavirus* in the family Coronaviridae (*5*–*7*). The SARS-CoV receptor is angiotensin-converting enzyme 2 (ACE2) (*8*, *9*). The spike proteins of both viruses bind to ACE2, whereas soluble ACE2 blocks infection by SARS-CoV and SARS-CoV-2 (*10*–*13*). Transmission of SARS-CoV-2 is thought to occur through respiratory droplets and fomites. The virus can be detected in upper respiratory tract samples, implicating the nasopharynx as a site of replication. In human lung, ACE2 is expressed mainly in alveolar epithelial type II cells and ciliated cells (*14*–*16*). However, the highest expression of ACE2 in the human body occurs in the brush border of intestinal enterocytes (*14*, *17*). Even though respiratory symptoms dominate the clinical presentation of COVID-19, gastrointestinal symptoms are observed in a subset of patients (*18*, *19*). Moreover, viral RNA can be found in rectal swabs even after nasopharyngeal testing has turned negative, implying gastrointestinal infection and a fecal–oral transmission route (*20*–*22*).

[1]Viroscience Department, Erasmus Medical Center, Rotterdam, Netherlands. [2]Oncode Institute, Hubrecht Institute, Royal Netherlands Academy of Arts and Sciences and University Medical Center, Utrecht, Netherlands. [3]The Maastricht Multimodal Molecular Imaging Institute, Maastricht University, Maastricht, Netherlands. [4]Center for Molecular Medicine and Oncode Institute, University Medical Centre Utrecht, Utrecht, Netherlands. [5]Hartwig Medical Foundation, Amsterdam, Netherlands.
*These authors contributed equally to this work.
†These authors contributed equally to this work.
‡Corresponding author. Email: h.clevers@hubrecht.eu (H.C.); b.haagmans@erasmusmc.nl (B.L.H.)

SARS-CoV-2 infects airway and gut organoids

Organoids are three-dimensional (3D) structures that can be grown from adult stem cells and recapitulate key aspects of the organ from which those cells derive. Because SARS-CoV and SARS-CoV-2 target the lung, we added virus to organoid-derived human airway epithelium cultured in 2D and observed that SARS-CoV and SARS-CoV-2 readily infected differentiated airway cultures. (Fig. 1A). Immunostaining reveal that the viruses targeted ciliated cells but not goblet cells (Fig. 1, B and C).

Human small intestinal organoids (hSIOs) are established from primary gut epithelial stem cells, can be expanded indefinitely in 3D culture, and contain all proliferative and differentiated cell types of the in vivo epithelium (*23*). hSIOs have also allowed the first in vitro culturing of norovirus (*24*). We exposed ileal hSIOs grown under four different culture conditions (EXP, DIF, DIF-BMP, and EEC) to SARS-CoV and SARS-CoV-2 at a multiplicity of infection of 1. hSIOs grown in Wnt high-expansion (EXP) medium overwhelmingly consisted of stem cells and enterocyte progenitors. Organoids grown in differentiation (DIF) medium contained enterocytes, goblet cells, and low numbers of enteroendocrine cells (EECs). The addition of BMP2/4 to DIF medium (DIF-BMP medium) led to further maturation (*25*). In the final condition (EEC), we induced the expression of NeuroG3 from a stably transfected vector with doxycycline to raise EEC numbers (fig. S3D). Samples were harvested at multiple time points after infection and processed for the analyses shown in Figs. 2 to 5. Both SARS-CoV and SARS-CoV-2 productively infected hSIOs, as assessed by quantitative reverse transcription polymerase chain reaction (qRT-PCR) for viral sequences and by live virus titrations on VeroE6 cells (see Fig. 2 for lysed organoids and fig. S1 for organoid supernatant). Infectious virus particles and viral RNA increased for both viruses in all conditions. Because EXP medium supported virus replication (Fig. 2, A and E), enterocyte progenitors appeared to be a primary viral target. Differentiated organoids (grown in DIF and DIF-BMP medium) produced slightly (nonstatistically significant) lower levels of

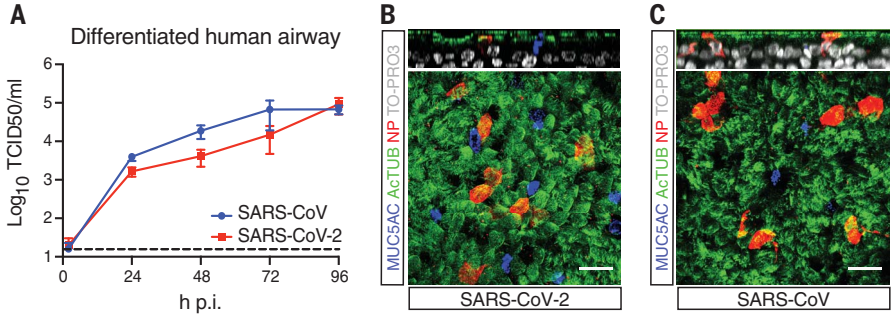

Fig. 1. SARS-CoV and SARS-CoV-2 infect 2D human airway cultures. (**A**) Live virus titers can be observed by virus titrations on VeroE6 cells of apical washes at 2, 24, 48, 72, and 96 h after infection with SARS-CoV (blue) and SARS-CoV-2 (red). The dotted line indicates the lower limit of detection. Error bars indicate SEM. $N = 4$. $^{*}P < 0.05$, $^{**}P < 0.01$, $^{***}P < 0.001$. (**B** and **C**) Immunofluorescent staining of SARS-CoV-2–infected (B) and SARS-CoV–infected (C) differentiated airway cultures. Nucleoprotein (NP) stains viral nucleocapsid (red), which colocalized with the ciliated cell marker AcTUB (green). Goblet cells are identified by MUC5AC (blue). Nuclei are stained with TO-PRO3 (white). Scale bars, 20 μM. Top panels are side views and bottom panels are top views.

infectious virus (Fig. 2 and fig. S1). In organoids induced to generate EECs, virus yields were similar to those in EXP medium (Fig. 2, D and H). In differentiated hSIOs, SARS-CoV-2 titers remained stable at 60 hours after infection, whereas SARS-CoV titers dropped by 1 to 2 log (Fig. 2, B, C, F, and G). The latter decline was not observed in infected hSIOs grown in EXP medium. Culture supernatants across culture conditions contained lower levels of infectious virus compared with lysed hSIOs, implying that virus was primarily secreted apically (fig. S1, A to D). Despite this, viral RNA was detected readily in culture supernatants, correlating with the infectious virus levels within hSIOs (Fig. 2, E to H, and fig. S1, E to H).

ACE2 mRNA expression differed greatly between the four conditions. EXP-hSIOs expressed 300-fold less ACE2 mRNA compared with DIF-hSIOs when analyzed in bulk (fig. S2). BMP treatment induced 6.5-fold up-regulation of ACE2 mRNA compared with DIF treatment alone. Because this did not yield infection rate differences, the DIF-BMP condition was not analyzed further.

SARS-CoV-2 infects enterocyte lineage cells

To determine the target cell type, we then performed confocal analysis on hSIOs cultured in EXP, DIF, or EEC conditions. We stained for viral double-stranded RNA (dsRNA), viral nucleocapsid protein, KI67 to visualize proliferative cells, actin (using phalloidin) to visualize enterocyte brush borders, and DNA (DAPI) and cleaved caspase 3 to visualize apoptotic cells. Generally, comparable rates of viral infections were observed in the organoids growing in all three conditions. We typically noted staining for viral components (white) in rare, single cells at 24 hours. At 60 hours, the number of infected cells had substantially increased (Fig. 3A). Infected cells invariably displayed proliferative enterocyte progenitor phenotypes (EXP; Fig. 3B, top) or ApoA1^{+} enterocyte phenotypes (DIF; Fig. 3B, bottom). SARS-CoV also readily infected enterocyte lineage cells (fig. S3, A and B), as was shown previously (*26*, *27*). Some infected enterocyte progenitors were in mitosis (fig. S3C). Whereas EEC organoids produced appreciable titers, we never observed infection of chromogranin-A^{+} EECs (fig. S3, D and E). We also did not observe infection of goblet cells across culture conditions. At 60 hours, apoptosis became prominent in both

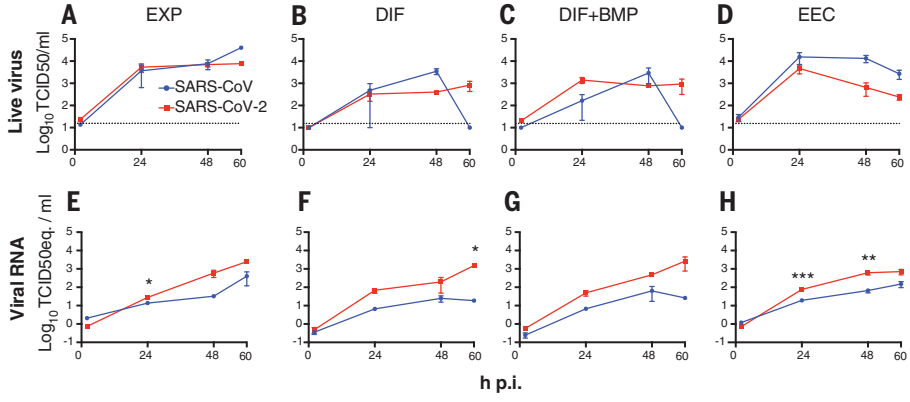

Fig. 2. SARS-CoV and SARS-CoV-2 replicate in hSIOs. (**A** to **D**) Live virus titers can be observed by virus titrations on VeroE6 cells of lysed organoids at 2, 24, 48, and 60 h after infection with SARS-CoV (blue) and SARS-CoV-2 (red). Different medium compositions show similar results. (**E** to **H**) qRT-PCR analysis targeting the E gene of similar time points and medium compositions as (A) to (D). The dotted line indicates the lower limit of detection. Error bars indicate SEM. $N = 3$. $^{*}P < 0.05$, $^{**}P < 0.01$, $^{***}P < 0.001$.

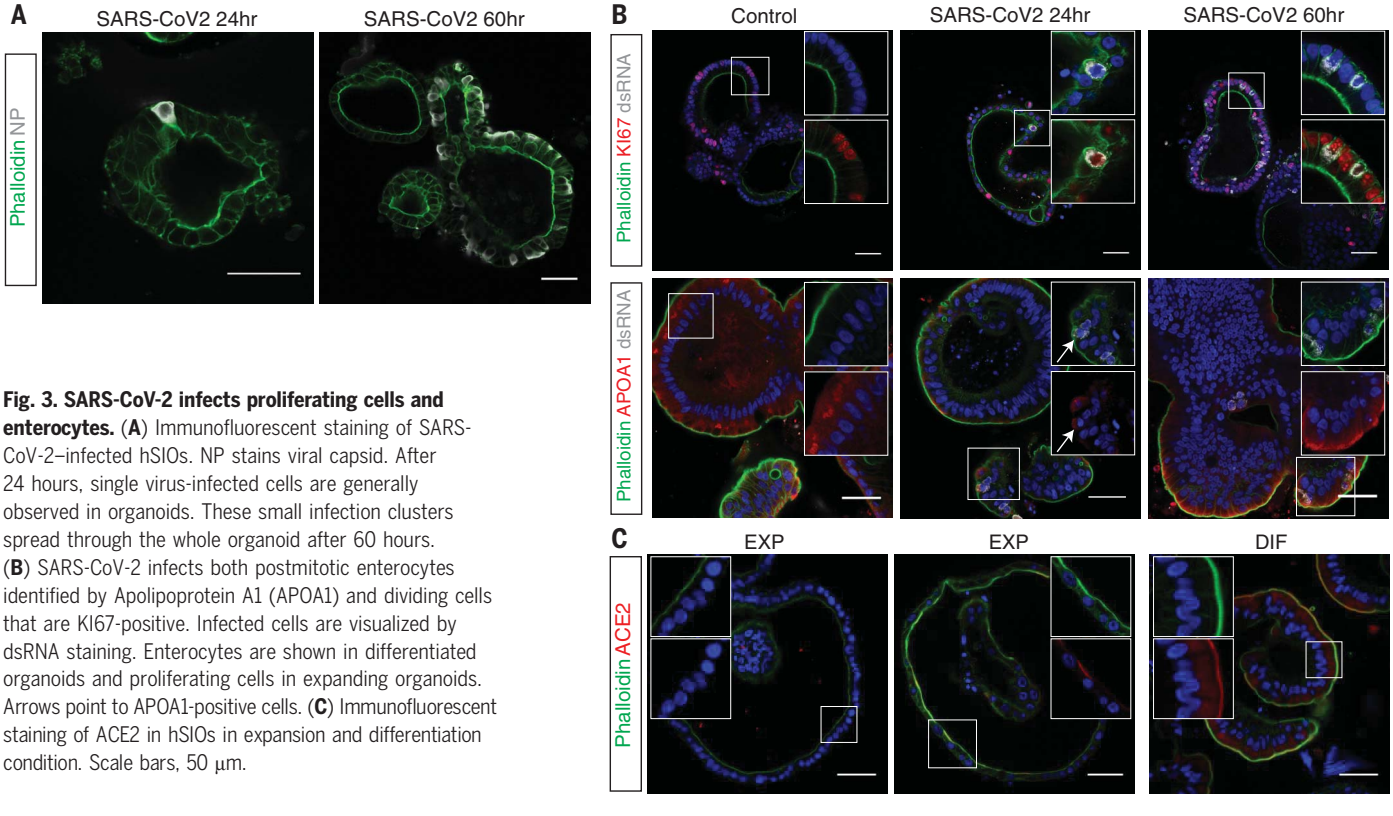

Fig. 3. SARS-CoV-2 infects proliferating cells and enterocytes. (**A**) Immunofluorescent staining of SARS-CoV-2–infected hSIOs. NP stains viral capsid. After 24 hours, single virus-infected cells are generally observed in organoids. These small infection clusters spread through the whole organoid after 60 hours. (**B**) SARS-CoV-2 infects both postmitotic enterocytes identified by Apolipoprotein A1 (APOA1) and dividing cells that are KI67-positive. Infected cells are visualized by dsRNA staining. Enterocytes are shown in differentiated organoids and proliferating cells in expanding organoids. Arrows point to APOA1-positive cells. (**C**) Immunofluorescent staining of ACE2 in hSIOs in expansion and differentiation condition. Scale bars, 50 μm.

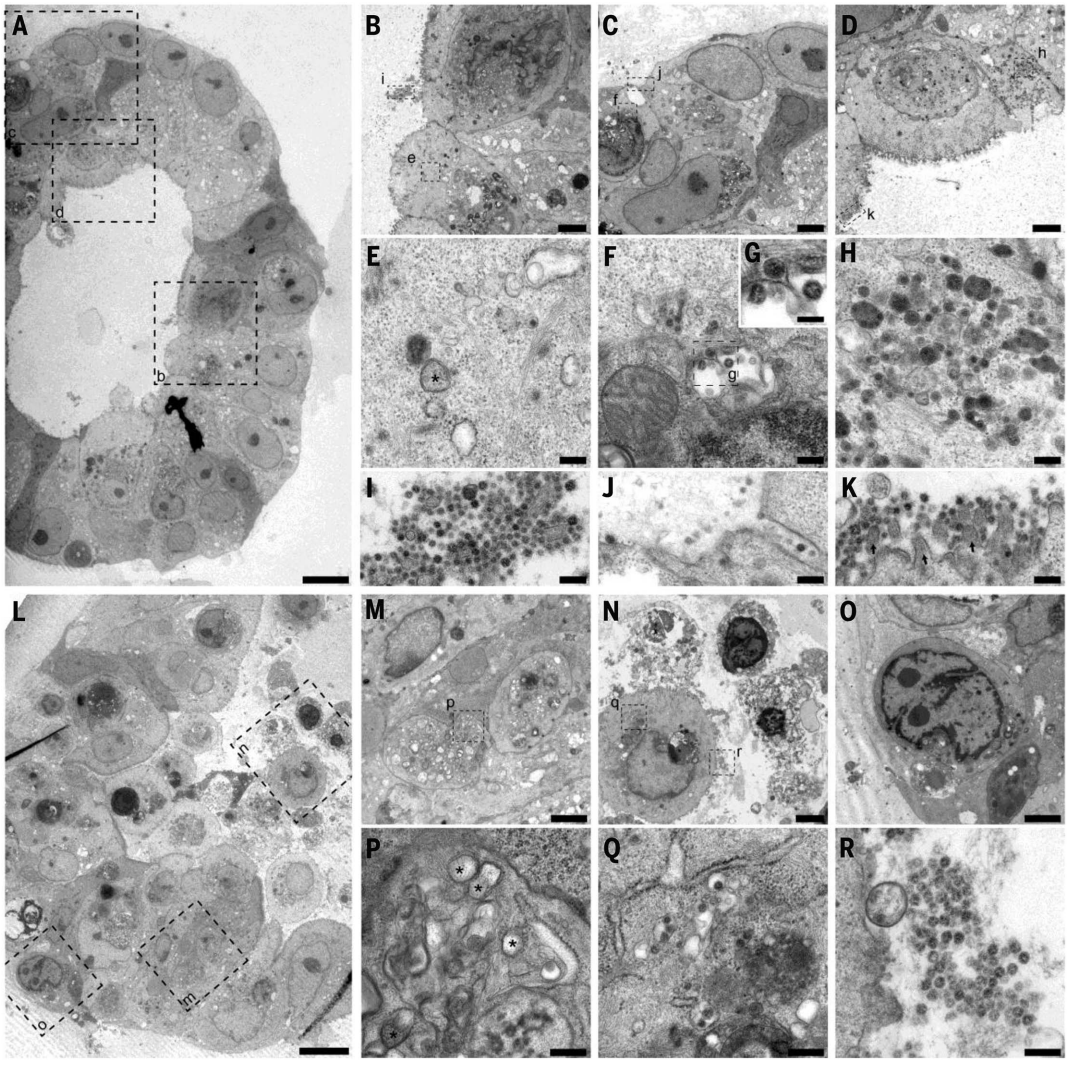

Fig. 4. Transmission electron microscopy analysis of SARS-CoV-2–infected intestinal organoids. (**A** to **H**) Overview of an intact organoid (A) showing the onset of virus infection [(B) to (D)] at different stages of the viral lifecycle, i.e., early double membrane vesicles (DMVs) [(E), asterisk], initial viral production in the Golgi apparatus [(F) and (G)], and complete occupation of virus particles inside the endomembrane system (H). (**I** to **K**) Extracellular viruses are observed in the lumen of the organoid (I) and are found at the basal side (J) and the apical side (K) alongside the microvilli (arrows). Scale bars, 10 μm (A), 2.5 μm [(B) to (D)], 250 nm [(E), (F), and (H) to (K)] and 100 nm (G). (**L** to **Q**) Overview of an organoid (L) showing severely infected cells [(M) and (O)], disintegrated cells (O), and stressed cells as evident from the atypical nucleoli (P). Intact cells reveal DMV areas of viral replication [(P), asterisks] and infected Golgi apparatus (Q). (**R**) Extracellular clusters of viruses. Scale bars, 10 μm (L), 2.5 μm [(M) to (P)], and 250 nm [(P) to (R)].

SARS-CoV– and SARS-CoV-2–infected enterocytes (fig. S5). ACE2 protein was readily revealed as a bright and ubiquitous brush border marker in hSIOs in DIF medium (Fig. 3C). In hSIOs in EXP medium, ACE2 staining was much lower, yet still apical, in occasional cells in a subset of organoids that displayed a more mature morphology (Fig. 3C). In immature (cystic) organoids within the same cultures, the ACE2 signal was below the detection threshold. The percentages of infected organoids under EXP and DIF conditions are given in fig. S4. Figure S5 shows images and quantification of apoptotic cells upon infection.

Ultrastructural analysis of the viral life cycle in enterocytes

Unsupervised transmission electron microscopy (*28*) was performed on selected highly infected samples. Figure 4 shows two hSIOs selected from 42 hSIOs imaged at 60 hours after SARS-CoV-2 infection. These differ in the state of infection: Whereas the cellular organization within organoid 1 was still intact (Fig. 4A, entire organoid; B to D, intermediate magnification; E to K, high magnification), many disintegrated cells can be seen in organoid 2 (Fig. 4, bottom; L, entire organoid; M to O, intermediate magnification; P to R, high magnification). Viral particles of 80 to 20 nm occurred in the lumen of the organoid (Fig. 4I) at the basolateral (Fig. 4J) and apical side (Fig. 4K) of enterocytes. Double-membrane vesicles, which are the subcellular site of viral replication (*29*), are visualized in Fig. 4, E and P. The nuclei in both organoids differed from nuclei in mock-infected organoids by having a slightly rounder shape. Other differences were that the nuclear contour index (*30*) was 4.0 ± 0.5 versus 4.3 ± 0.5 for the control set, and there was more heterochromatin (Fig. 4N) and one or two dense nucleoli in the center (Fig. 4O).

RNA expression changes in infected enterocytes

We then performed mRNA-sequencing analysis to determine gene expression changes induced by SARS-CoV and SARS-CoV-2-infection of hSIOs cultured continuously in EXP medium and hSIOs cultured in DIF medium. Infection with SARS-CoV-2 elicited a broad signature of cytokines and interferon (IFN)–stimulated genes (ISGs) attributed to type I and III IFN responses (Fig. 5A and tables S1 and S2), as confirmed by gene ontology analysis (Fig. 5B). An overlapping list of genes appeared in SARS-CoV-2–infected DIF organoids (fig. S6 and table S3). mRNA-sequencing analysis confirmed differentiation of DIF organoids into multiple intestinal lineages, including ACE2 up-regulation (fig. S7). SARS-CoV also induced ISGs but to a much lower level (table S4). Figure 5C shows the regulation of SARS-CoV-2–induced genes in SARS-CoV–infected organoids. This induction was similar to infections with other viruses such as norovirus (*31*), rotavirus (*32*), and enteroviruses (*33*, *34*). A recent study (*35*) described an antiviral signature induced in human cell lines after SARS-CoV-2 infection. Whereas the ISG response was broader in hSIOs, the induced gene sets were in close agreement between the two datasets (fig. S8).

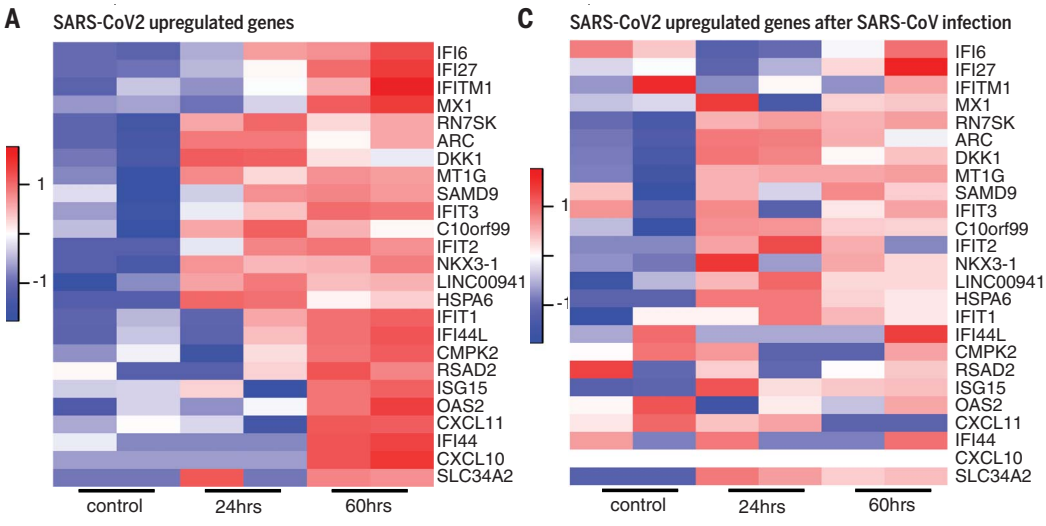

B

	ID	Name	P value
1	GO:0051607	defense response to virus	3.568E-24
2	GO:0009615	response to virus	2.325E-23
3	GO:0071357	cellular response to type I interferon	2.687E-18
4	GO:0060337	type I interferon signaling pathway	2.687E-18
5	GO:0034340	response to type I interferon	4.515E-18

Fig. 5. Transcriptomic analysis of SARS-CoV-2–infected intestinal organoids. (**A**) Heatmaps depicting the 25 most significantly enriched genes upon SARS-CoV-2 infection in expanding intestinal organoids. (**B**) Colored bar represents the *Z*-score of log2-transformed values. Shown is the gene ontology term enrichment analysis for biological processes of the 50 most significantly up-regulated genes upon SARS-CoV-2 infection in intestinal organoids. (**C**) Heatmaps depicting the genes from (A) in SARS-CoV–infected expanding organoids. Colored bar represents the *Z*-score of log2-transformed values.

One obvious similarity was the low expression of type I and III IFNs: We only noticed a small induction of the type III IFN IFNL1 in SARS-CoV-2–infected organoids. In SARS-CoV–infected organoids, we did not observe any type I or type III IFN induction. We confirmed these findings by enzyme-linked immunosorbent assay (ELISA) on the culture supernatant and qRT-PCR on extracted RNA of the hSIOs, which in addition to IFNL1, picked up low levels of type I IFN IFNB1 in SARS-CoV-2– but not in SARS-CoV–infected organoids (fig. S9). The specific induction of IP-10/CXCL10 and ISG15 by SARS-CoV-2 was also confirmed by ELISA and qRT-PCR, respectively (fig. S10). As in a previous study (*35*), a few cytokine genes were induced by both viruses, albeit to modest levels. For a comparison with (*35*), see fig. S11. Altogether, these data indicate that SARS-CoV-2 induces a stronger IFN response than SARS-CoV in hSIOs.

Finally, the infection was repeated in a second experiment in the same ileal hSIO line and analyzed after 72 hours. Analysis involved viral titration (fig. S12), confocal imaging (fig. S13), and mRNA sequencing (fig. S14). This experiment essentially confirmed the observations presented above. A limited, qualitative experiment applying confocal analysis demonstrated the infectability of two other lines available in the laboratory (one ileal and one duodenal) from independent donors (fig. S13). This study shows that SARS-CoV and SARS-CoV-2 infect enterocyte lineage cells in an hSIO model. We observed similar infection rates of enterocyte precursors and enterocytes, whereas ACE2 expression increased ~1000-fold upon differentiation at the mRNA level (fig. S2). This suggests that low levels of ACE2 may be sufficient for viral entry.

SARS-CoV-2 is the third highly pathogenic coronavirus (after SARS-CoV and MERS-CoV) to jump to humans within <20 years, suggesting that new zoonotic coronavirus spillovers are likely to occur in the future. Despite this, limited information is available on coronavirus pathogenesis and transmission, in part because of the lack of in vitro cell models that accurately model host tissues. Very recently, it was shown that human induced pluripotent stem cells differentiated toward a kidney fate supported replication of SARS-CoV-2 (*13*). Our data suggest that human organoids represent faithful experimental models with which to study the biology of coronaviruses.

REFERENCES AND NOTES

1. C. Drosten *et al.*, *N. Engl. J. Med.* **348**, 1967–1976 (2003).
2. W. J. Guan *et al.*, *N. Engl. J. Med.* **382**, 1708–1720 (2020).
3. S. Jiang, L. Du, Z. Shi, *Emerg. Microbes Infect.* **9**, 275–277 (2020).
4. N. Zhu *et al.*, *N. Engl. J. Med.* **382**, 727–733 (2020).
5. K. G. Andersen, A. Rambaut, W. I. Lipkin, E. C. Holmes, R. F. Garry, *Nat. Med.* **26**, 450–452 (2020).
6. R. Lu *et al.*, *Lancet* **395**, 565–574 (2020).
7. A. E. Gorbalenya *et al.*, *Nat. Microbiol.* **5**, 536–544 (2020).
8. Y. Imai *et al.*, *Nature* **436**, 112–116 (2005).
9. K. Kuba *et al.*, *Nat. Med.* **11**, 875–879 (2005).
10. A. C. Walls *et al.*, *Cell* **181**, 281–292.e6 (2020).
11. Y. Wan, J. Shang, R. Graham, R. S. Baric, F. Li, *J. Virol.* **94**, e00127-20 (2020).
12. D. Wrapp *et al.*, *Science* **367**, 1260–1263 (2020).
13. V. Monteil *et al.*, *Cell* 10.1016/j.cell.2020.04.004 (2020).
14. F. Qi, S. Qian, S. Zhang, Z. Zhang, *Biochem. Biophys. Res. Commun.* **526**, 135–140 (2020).
15. Y. Zhao, Z. Zhao, Y. Wang, Y. Zhou, Y. Ma, W. Zuo, Single-cell RNA expression profiling of ACE2, the receptor of SARS-CoV-2. bioRxiv 2020.01.26.919985 [Preprint]. 9 April 2010. https://doi.org/10.1101/2020.01.26.919985.
16. H. P. Jia *et al.*, *J. Virol.* **79**, 14614–14621 (2005).
17. The Human Protein Atlas, ACE2 protein expression summary (2020); https://www.proteinatlas.org/ENSG00000130234-ACE2.
18. J. Gu, B. Han, J. Wang, *Gastroenterology* **158**, 1518–1519 (2020).
19. G. Cholankeril *et al.*, *Gastroenterology* 10.1053/j.gastro.2020.04.008 (2020).
20. W. Wang *et al.*, *JAMA* (2020). 10.1001/jama.2020.3786
21. M. L. Holshue *et al.*, *N. Engl. J. Med.* **382**, 929–936 (2020).
22. F. Xiao *et al.*, *Gastroenterology* S0016-5085(20)30282-1 (2020). 10.1053/j.gastro.2020.02.055
23. T. Sato *et al.*, *Gastroenterology* **141**, 1762–1772 (2011).
24. K. Ettayebi *et al.*, *Science* **353**, 1387–1393 (2016).
25. J. Beumer *et al.*, *Nat. Cell Biol.* **20**, 909–916 (2018).
26. W. K. Leung *et al.*, *Gastroenterology* **125**, 1011–1017 (2003).
27. W. S. Chan *et al.*, *Mod. Pathol.* **18**, 1432–1439 (2005).
28. F. G. A. Faas *et al.*, *J. Cell Biol.* **198**, 457–469 (2012).
29. K. Knoops *et al.*, *PLOS Biol.* **6**, e226 (2008).
30. N. S. McNutt, W. R. Crain, *Cancer* **47**, 698–709 (1981).
31. M. Hosmillo *et al.*, *mBio* **11**, e00215-20 (2020).
32. K. Saxena *et al.*, *Proc. Natl. Acad. Sci. U.S.A.* **114**, E570–E579 (2017).
33. C. G. Drummond *et al.*, *Proc. Natl. Acad. Sci. U.S.A.* **114**, 1672–1677 (2017).
34. C. Good, A. I. Wells, C. B. Coyne, *Sci. Adv.* **5**, eaau4255 (2019).
35. D. Blanco-Melo *et al.*, *Cell* 10.1016/j.cell.2020.04.026 (2020).

ACKNOWLEDGMENTS

We thank E. Eenjes and R. Rottier for providing human lung material, A. de Graaff and the Hubrecht Imaging Centre (HIC) for microscopy assistance, Single Cell Discoveries for RNA library preparation, and the Utrecht Sequencing Facility (subsidized by the University Medical Center Utrecht, Hubrecht Institute, Utrecht University and NWO project 184.034.019). **Funding:** This work was supported by ERC Advanced Grant 67013 and by Lung Foundation

Netherlands to H.C. and by NWO Grant 022.005.032. K.K., J.Q.D., P.J.P., and R.B.G.R. received funding from the Dutch Technology Foundation STW (UPON 14207) and from European Union's Horizon 2020 Programme (grant no. 766970 Q-SORT). **Author contributions:** M.L., J.B., and J.V. performed experiments and designed the study. K.K. and J.Q.D. prepared samples. K.K. and R.B.G.R. performed imaging. K.K., J.P.v.S., P.J.P., and R.G.B.R. interpreted results. T.B., A.M., S.R., D.S., and M.G. measured virus titers. J.P. analyzed RNA-sequencing data. E.C. performed sequencing. M.K., B.H., and H.C. supervised the project. **Competing interests:** H.C. is an inventor on patents held by the Royal Netherlands Academy of Arts and Sciences that cover organoid technology (PCT/NL2008/050543, WO2009/022907; PCT/NL2010/000017, WO2010/090513; PCT/IB2011/002167, WO2012/014076; PCT/IB2012/052950, WO2012/168930;PCT/EP2015/060815, WO2015/173425; PCT/EP2015/077990, WO2016/083613; PCT/EP2015/077988, WO2016/083612; PCT/EP2017/054797,WO2017/149025; PCT/EP2017/065101, WO2017/220586; PCT/EP2018/086716, and GB1819224.5). H.C.'s full disclosure is given at https://www.uu.nl/staff/JCClevers/. **Data and materials availability:** Organoid lines may be requested directly from the nonprofit HUB (https://huborganoids.nl/), which does not directly benefit from this research. RNA-sequencing data can be accessed through GEO GSE149312. Data were deposited to the Image Data Resource (https://idr.openmicroscopy.org) under accession number idr0083.

SUPPLEMENTARY MATERIALS

science.sciencemag.org/content/369/6499/50/suppl/DC1
Materials and Methods
Figs. S1 to S14
Tables S1 to S4
References (*36*–*44*)
MDAR Reproducibility Checklist

View/request a protocol for this paper from *Bio-protocol*.

9 April 2020; accepted 29 April 2020
Published online 1 May 2020
10.1126/science.abc1669

Science

SARS-CoV-2 productively infects human gut enterocytes

Mart M. Lamers, Joep Beumer, Jelte van der Vaart, Kèvin Knoops, Jens Puschhof, Tim I. Breugem, Raimond B. G. Ravelli, J. Paul van Schayck, Anna Z. Mykytyn, Hans Q. Duimel, Elly van Donselaar, Samra Riesebosch, Helma J. H. Kuijpers, Debby Schipper, Willine J. van de Wetering, Miranda de Graaf, Marion Koopmans, Edwin Cuppen, Peter J. Peters, Bart L. Haagmans and Hans Clevers

Science **369** (6499), 50-54.
DOI: 10.1126/science.abc1669originally published online May 1, 2020

Intestinal organoids as an infection model

Severe acute respiratory syndrome coronavirus 2 (SARS-CoV-2) causes an influenza-like disease with a respiratory transmission route; however, patients often present with gastrointestinal symptoms such as diarrhea, vomiting, and abdominal pain. Moreover, the virus has been detected in anal swabs, and cells in the inner-gut lining express the receptor that SARS-CoV-2 uses to gain entry to cells. Lamers *et al.* used human intestinal organoids, a "mini-gut" cultured in a dish, to demonstrate that SARS-CoV-2 readily replicates in an abundant cell type in the gut lining —the enterocyte—resulting in the production of large amounts of infective virus particles in the intestine. This work demonstrates that intestinal organoids can serve as a model to understand SARS-CoV-2 biology and infectivity in the gut.

Science, this issue p. 50

Science (print ISSN 0036-8075; online ISSN 1095-9203) is published by the American Association for the Advancement of Science, 1200 New York Avenue NW, Washington, DC 20005. The title *Science* is a registered trademark of AAAS.

Science (print ISSN 0036-8075; online ISSN 1095-9203) is published by the American Association for the Advancement of Science, 1200 New York Avenue NW, Washington, DC 20005. The title *Science* is a registered trademark of AAAS.